
Princeton Plasma Physics Laboratory

PPPL-

PPPL-



Prepared for the U.S. Department of Energy under Contract DE-AC02-09CH11466.

Princeton Plasma Physics Laboratory

Report Disclaimers

Full Legal Disclaimer

This report was prepared as an account of work sponsored by an agency of the United States Government. Neither the United States Government nor any agency thereof, nor any of their employees, nor any of their contractors, subcontractors or their employees, makes any warranty, express or implied, or assumes any legal liability or responsibility for the accuracy, completeness, or any third party's use or the results of such use of any information, apparatus, product, or process disclosed, or represents that its use would not infringe privately owned rights. Reference herein to any specific commercial product, process, or service by trade name, trademark, manufacturer, or otherwise, does not necessarily constitute or imply its endorsement, recommendation, or favoring by the United States Government or any agency thereof or its contractors or subcontractors. The views and opinions of authors expressed herein do not necessarily state or reflect those of the United States Government or any agency thereof.

Trademark Disclaimer

Reference herein to any specific commercial product, process, or service by trade name, trademark, manufacturer, or otherwise, does not necessarily constitute or imply its endorsement, recommendation, or favoring by the United States Government or any agency thereof or its contractors or subcontractors.

PPPL Report Availability

Princeton Plasma Physics Laboratory:

<http://www.pppl.gov/techreports.cfm>

Office of Scientific and Technical Information (OSTI):

<http://www.osti.gov/bridge>

Related Links:

[U.S. Department of Energy](#)

[Office of Scientific and Technical Information](#)

[Fusion Links](#)

Importance of plasma response to non-axisymmetric perturbations in tokamaks

Jong-kyu Park,¹

Allen H. Boozer,² Jonathan E. Menard,¹

Andrea M. Garofalo,³ Michael J. Schaffer,³ Richard J. Hawryluk,¹ Stanley M. Kaye,¹ Stefan P. Gerhardt,¹ Steve A. Sabbagh,² and the NSTX team¹

¹*Princeton Plasma Physics Laboratory, Princeton, New Jersey, NJ 08543*

²*Department of Applied Physics and Applied Mathematics,*

Columbia University, New York, NY 10027

³*General Atomics, San Diego, CA 92186*

(Dated: April 21, 2009)

Abstract

Tokamaks are sensitive to deviations from axisymmetry as small as $\delta B/B_0 \sim 10^{-4}$. These non-axisymmetric perturbations greatly modify plasma confinement and performance by either destroying magnetic surfaces with subsequent locking or deforming magnetic surfaces with associated non-ambipolar transport. The Ideal Perturbed Equilibrium Code (IPEC) calculates ideal perturbed equilibria and provides important basis for understanding the sensitivity of tokamak plasmas to perturbations. IPEC calculations indicate that the ideal plasma response, or equivalently the effect by ideally perturbed plasma currents, is essential to explain locking experiments on National Spherical Torus eXperiment (NSTX) and DIII-D. The ideal plasma response is also important for Neoclassical Toroidal Viscosity (NTV) in non-ambipolar transport. The consistency between NTV theory and magnetic braking experiments on NSTX and DIII-D can be improved when the variation in the field strength in IPEC is coupled with generalized NTV theory. These plasma response effects will be compared with the previous vacuum superpositions to illustrate the importance. However, plasma response based on ideal perturbed equilibria is still not sufficiently accurate to predict the details of NTV transport, and can be inconsistent when currents associated with a toroidal torque become comparable to ideal perturbed currents.

I. INTRODUCTION

Tokamaks confine toroidal plasmas in a magnetic field that is almost axisymmetric. However, a significant degradation of performance in tokamak plasmas are observed for non-axisymmetric magnetic perturbations as small as $\delta B/B_0 \sim 10^{-4}$. [1–6]. Tokamaks are difficult to build without such small errors. Interestingly, such a small magnetic asymmetries can be beneficial. Recent experiments on Edge Localized Modes (ELMs) have shown that non-axisymmetry as small as $\delta B/B_0 \sim 10^{-4}$ can eliminate or modify ELMs [7–9], which is critical for avoiding severe damages to plasma-facing components. These observations indicate that tokamaks are very sensitive to small non-axisymmetric perturbations, and thus must be controlled at the $\delta B/B_0 \sim 10^{-4}$ level for optimal tokamak plasma performance.

A standard approximation is to superpose a non-axisymmetric external field $\delta\vec{B}^x$ onto the \vec{B}_0 of an axisymmetric tokamak equilibrium. This approximation essentially assumes that the plasma response, or equivalently the field $\delta\vec{B}^p$ from perturbed plasma currents, is much smaller or at most comparable to the external field $\delta\vec{B}^x$ driven by external currents. This assumption often fails and thus the field due to perturbed plasma currents $\delta\vec{B}^p$ must be included in the *total field*, $\delta\vec{B} = \delta\vec{B}^x + \delta\vec{B}^p$. The magnetic field due to the plasma response can either amplify or shield the external field, and is essential for understanding the sensitivity of tokamaks to small non-axisymmetric perturbations.

The plasma response to external perturbations can be understood based on three dimensional plasma equilibria. The external perturbations change for slower Alfvén time, which is time scale for the relaxation to an equilibrium. In three dimensional equilibria, the nested magnetic surfaces are non-axisymmetrically deformed, or destroyed by the opening of magnetic islands near the rational surfaces. If islands exist, however, plasma rotation slows and can lock to the islands via multiple mechanisms [10–14], which often leads to a plasma disruption. The destruction of magnetic surfaces by external magnetic perturbations must be negligibly small in the bulk of the plasma. Before the onset of the significant islands and plasma locking, the distortion of the plasma by external magnetic perturbations can be effectively described by ignoring the islands at the rational surfaces. This is consistent with the constraints in ideal MagnetoHydroDynamics (MHD), which does not allow topological changes in magnetic field such as magnetic islands. Therefore, the fundamental and the practically important level of understanding for the plasma response can be achieved by

studying ideal perturbed equilibria.

In ideal perturbed equilibria, there are two important consequences [15, 16]: (1) Parallel currents shield the normal resonant field δB_{mn} at the rational surfaces, which is driving the opening of an island, and (2) the deformation of magnetic surfaces causes non-ambipolar transport [17–22] due to the symmetry-breaking of the magnetic field strength $|B|$. In particular, toroidal torque by non-ambipolar transport is associated with Neoclassical Toroidal Viscosity (NTV) [14, 23–25].

This paper will describe the calculations of ideal perturbed equilibria (Sec. II), give a brief review of its applications to plasma locking through δB_{mn} (Sec. III), and to the NTV torque through non-axisymmetries in $|B|$ (Sec. IV). Comparisons will be made with the vacuum superposition approximations to show the importance of the plasma response. The plasma response based on ideal perturbed equilibria, however, is valid only for an order-of-magnitude prediction for NTV torque and is not fully self-consistent. Both δB_{mn} and non-axisymmetries in $|B|$ cause a toroidal torque, but the currents associated with a toroidal torque are not included in ideal perturbed equilibria. This will be briefly discussed (Sec. V).

II. IDEAL PERTURBED EQUILIBRIUM

The Ideal Perturbed Equilibrium Code (IPEC) [26], which is based on the DCON [27] and the VACUUM [28] stability codes, solves free-boundary ideal perturbed equilibria preserving the pressure $p(\psi)$ and the safety factor $q(\psi)$ profiles. The fixed $q(\psi)$ profile means that no topological changes in magnetic field lines are allowed, so magnetic islands are always shielded. IPEC solves the perturbed force balance equation

$$\vec{F} = \vec{0} = \vec{\nabla}\delta p - \delta\vec{j} \times \vec{B}_0 - \vec{j}_0 \times \delta\vec{B}, \quad (1)$$

with the constraint at each $q = m/n$ rational surface that the resonant magnetic perturbation vanish,

$$\Phi_{mn} = \frac{1}{(2\pi)^2} \oint d\vartheta \oint d\varphi \mathcal{J} \delta\vec{B} \cdot \vec{\nabla}\psi e^{-i(m\vartheta - n\varphi)} = 0, \quad (2)$$

where \mathcal{J} is the Jacobian of magnetic coordinates $(\psi, \vartheta, \varphi)$. This constraint eliminates magnetic islands at the rational surfaces, and produces a jump in the tangential field across the

rational surfaces. The surface current associated with this jump gives, within a sign, the resonant magnetic perturbation that is trying to drive an island.

The external boundary conditions are given by the external perturbation, $\delta\vec{B}^x \cdot \hat{n}_b$, normal to a control surface, or equivalently to the plasma boundary. As described in detail in [26], the total normal field on the plasma boundary can be determined as $\delta\vec{B} \cdot \hat{n}_b = \hat{P}[\delta\vec{B}^x \cdot \hat{n}_b]$ with a permeability operator \hat{P} . IPEC uses virtual surface currents to construct the permeability operator, and gives the total normal field on the boundary surface as well as all the components of the total perturbed field and displacement, $(\delta\vec{B}(\vec{x}), \vec{\xi}(\vec{x}))$, which include the plasma response throughout the plasma volume.

Perturbed plasma currents including shielding currents at the rational surfaces can often significantly modify the penetration of the field. This can be easily illustrated with a cylindrical and force-free (or zero pressure, $p = 0$) example. Consider a cylindrical plasma with the $q = 2$ resonant surface at $r/a \sim 0.8$ with a minor radius. The plasma is enclosed by a conformal wall located at $r/a = 1.2$, and the external perturbations are specified by external currents in this wall. A perturbed equilibrium without the plasma can be obtained using vacuum superposition, and a perturbed equilibrium with the plasma can be obtained using IPEC. Also, one can obtain a perturbed equilibrium with the plasma using the cylindrical force-free equilibrium equation. The perturbed magnetic field for the cylindrical plasma is written as $\delta\vec{B} = \vec{\nabla}\delta A_{\parallel} \times \hat{z} = \hat{r}(1/r)(\partial\delta A_{\parallel}/\partial\theta) - \hat{\theta}(\partial\delta A_{\parallel}/\partial r)$. With a perturbation $\delta A_{\parallel} = \delta A_{\parallel} \cos(m\theta - nz/R)$, the perturbed equilibrium is [29]

$$\frac{1}{r} \frac{d}{dr} \left(r \frac{d\delta A_{\parallel}}{dr} \right) - \frac{m^2 \delta A_{\parallel}}{r^2} = \frac{q}{r} \frac{m}{m - nq} \frac{d}{dr} (K) \delta A_{\parallel}, \quad (3)$$

given a current profile $K(r) = \mu_0 j_{\parallel}(r)/B_0$. A simple numerical routine, *Cylinder forcefree*, was developed to solve Eq. (3).

Fig. 1 shows each ($m = 2, n = 1$) perturbed equilibrium in terms of the normal field, using vacuum superposition, IPEC and Cylinder force-free. The IPEC case is obtained for a near cylindrical ($\epsilon \equiv a/R = 0.1$) and near force-free ($\beta_N \equiv \beta_t/(aB_{T0}/I_p) = 0.1$, where β_t is the toroidal β , B_{T0} is the toroidal field at the magnetic axis, and I_p is the plasma current) plasma. From Fig. 1, one can see that the IPEC solution using virtual surface currents is almost identical to the Cylinder force-free solution inside the plasma. The benchmark of the IPEC solution in the cylindrical limit has been done in this way. Compared to the vacuum superposition, the ideally perturbed equilibrium (by either of the IPEC or the Cylinder force-

free solution) shows a fundamental difference in the penetration of the field. The normal field is completely shielded inside the resonant surface, and the jump in the derivative of normal field implies the existence of currents shielding the resonant magnetic field. Also, perturbed plasma currents including these shielding currents significantly change the profile of the magnetic field compared with the vacuum magnetic field.

Amplification instead of shielding also can be easily found in the cylindrical force-free example. Fig. 2 illustrates the solutions for this case using vacuum superposition, IPEC, and Cylinder force-free by applying $(m = 3, n = 1)$ external currents at the wall. Since the resonant $q = 3$ surface is close to, but outside the plasma boundary ($r/a \sim 1.04$), plasma is close to instabilities associated with $(m = 3, n = 1)$ and the energy required to perturb plasma is very small [30]. In addition to shielding and amplification, tokamak plasmas have strong toroidicity, and thus strong poloidal harmonic coupling. This coupling can also greatly change the perturbed field and displacement from what would be expected from vacuum superposition.

III. DESTRUCTION OF FLUX SURFACES AND PLASMA LOCKING

The inclusion of plasma response gives a correct physical interpretation for a locking. When plasma is almost ideal before the onset of a locking, magnetic islands are suppressed by shielding currents at the rational surfaces. However, there is an upper limit of perturbation amplitudes, where the electromagnetic torque becomes too strong for a rotating plasma to maintain the shielding currents. This is often called *error field penetration* [10–13]. The balance between the electromagnetic torque by shielding currents and the viscous torque by plasma rotation is determined by the inner-layer dynamics, but shielding currents must be determined from the outer-layer, or equivalently a perturbed equilibrium. IPEC gives shielding currents before the balance is lost and thus when islands can be ignored.

The shielding currents give the resonant field driving magnetic islands, which can be called the *total resonant field*, δB_{mn} at $q = m/n$, compared to the *external resonant field*, δB_{mn}^x obtained by vacuum superposition. The total resonant field can be obtained using $\vec{\nabla} \times \vec{B} = \mu_0 \vec{j}_s$ with the shielding current \vec{j}_s , which suppresses the total resonant field. The external resonant field penetrates without distortions by perturbed plasma currents and thus can be directly obtained by the resonant component of the field at the rational surfaces.

The total and external resonant field would be linear if the applied field spectrum is fixed, and even can be very similar in the cylindrical force-free plasmas. However, the relation is more complicated in tokamak plasmas, because of shielding or amplification, and poloidal harmonic coupling. Experiments have found that the critical amplitudes of the external field or the external current are approximately linear with locking densities [1–6], and also some theories have expected the positive correlation between the critical field and the locking density [10–13]. However, the approximation of the external resonant field for the resonant field driving islands has been often unsuccessful to find the correlation. An alternative method such as three-mode coupling scheme [3, 4] has been proposed to account for poloidal harmonic coupling, but recent error field correction experiments in National Spherical Torus eXperiment (NSTX) [31] and DIII-D [32] have shown the irrelevance of such vacuum approximations [33].

IPEC applications to the intrinsic error correction have highlighted the importance of the total resonant field, and thus in general the importance of the plasma response. As shown in [33] and Figs. 3 and 4, consistent correlations were restored between the total resonant field and the locking density, for the cases where the external resonant field showed no correlations or even opposite results in both NSTX and DIII-D. Also, the strong correlations among the total resonant resonant field δB_{mn} (δB_{21} and δB_{31} in Fig. 4) at different rational surfaces imply that the plasma response is sensitive to a particular external field [33, 34]. However, the estimations of the total resonant field have been improved from [33] as explained in the following paragraphs.

The first issue comes from the magnitude of the resonant field δB_{mn} or δB_{mn}^x depending on the choice of magnetic coordinates. The difference can often be large as shown in [35], but a physical quantity such as the size of magnetic islands must be invariant. Nevertheless, it is still useful to represent a physical quantity by a relevant number of Gauss, and so one can be define the *weighted total (external) resonant field* as

$$\delta B_{mn}^{(x)} = \frac{\oint e^{-i(m\vartheta - n\varphi)} \delta \vec{B} \cdot d\vec{a}}{\oint da}, \quad (4)$$

where $d\vec{a}$ is the surface area vector normal to the rational surface and $d\vec{a} = d\vartheta d\varphi \mathcal{J} \vec{\nabla} \psi$. This definition makes the resonant component, $m/n = q$, independent of the choice of magnetic coordinates. Even though the number of Gauss of the weighted resonant field is not an amplitude of an actual magnetic field, the weighted resonant field is directly proportional to

Δ^2 , where Δ is the size of an island [29, 35]. If one uses Fourier decomposition for the total (external) resonant field in magnetic coordinates as,

$$\delta B_{mn}^{(x),Coord} = \frac{1}{(2\pi)^2} \oint \oint e^{-i(m\vartheta - n\varphi)} (\delta \vec{B} \cdot \hat{n}) d\vartheta d\varphi, \quad (5)$$

then this quantity can include non-resonant components that are irrelevant for islands. Here the superscript *Coord* indicates a set of magnetic coordinates, and here so-called PEST coordinates [36] will be used for comparison. PEST coordinates are easy in practice since they are based on an ordinary toroidal angle $\varphi = \phi$.

Fig. 3 shows the revised analysis of NSTX $n = 1$ corrections in [33] using the weighted δB_{21} , δB_{21}^x and $\delta B_{21}^{x,PEST}$. The blue box indicates the empirically determined optimal toroidal phase of $n = 1$ correction field by Error Field Correction (EFC) coils to mitigate a locking [37], and thus one would expect the reduced resonant field at the optimal phase. However, the external resonant field in PEST magnetic coordinates $\delta B_{21}^{x,PEST}$ can give the opposite results as shown in [33]. When one calculates the weighted external and total resonant field, δB_{21}^x and δB_{21} , the results become consistent. The total resonant field was consistent in [33], where the results were based on Hamada coordinates [38] δB_{21}^{Hamada} , even without the weighting factor since it used the shielding currents \vec{j}_s that are independent of magnetic coordinates. Nonetheless, the total resonant field given by $\vec{\nabla} \times \delta \vec{B} = \mu_0 \vec{j}_s$ also must be represented by the weighted form as shown in Fig. 3.

The NSTX examples show that the weighted δB_{mn}^x may approximate the weighted δB_{mn} . However, DIII-D $n = 1$ corrections showed that the weighted δB_{mn}^x can differ greatly from the weighted δB_{mn} in Fig. 4. Here the same experiments in [33] are presented, but with the weighted δB_{mn} . In addition, Fig. 4 has more corrections. IPEC calculation uses $\delta \vec{B} \cdot \hat{n}_b = \vec{P}[\delta \vec{B}^x \cdot \hat{n}_b]$ on the plasma boundary in a chosen system of magnetic coordinates based on Eq. (5), but the previous analysis [33] used the spectrum of the weighted external field on the boundary based on Eq. (4) in PEST coordinates. This weighted spectral analysis has been used in DIII-D since 2004 to obtain the invariant resonant field for islands [39]. Although the weighted resonant field is invariant, other weighted components depend on the choice of magnetic coordinates [35]. The revised calculations in Fig. 4 removed the weighting factor on the boundary to have the correct interface through $\delta \vec{B} \cdot \hat{n}_b = \vec{P}[\delta \vec{B}^x \cdot \hat{n}_b]$ in IPEC. Also, it is found that IPEC results can be unreliable when an internally unstable $q = 1$ surface exists, so the $q = 1$ surfaces close to the magnetic axis are ignored by enforcing

$q_0 \gtrsim 1$ at the magnetic axis in the given axisymmetric equilibria. Note that amplification is not as strong as the previous report in [33].

The confusion between the spectra of the field in Eqs. (4) and (5) occurred since they become identical in a cylinder for all the components in any set of magnetic coordinates. However, the differences are large in tokamak plasmas, so it is important to use the weighted form to obtain the correct resonant component of the field. The weighted external resonant field δB_{mn}^x includes some of geometrical poloidal coupling, so it can improve the prediction based on vacuum approximation, as shown in Fig. 3. It may be similar to the previous method using three-mode coupling scheme [3, 4] based on the external resonant field $\delta B_{mn}^{x,PEST}$. However, these vacuum approximations can be still inaccurate by neglecting the plasma response, that is, the contribution of the field by perturbed plasma currents $\delta \vec{B}^p$, as demonstrated in Fig. 4. The plasma response can be given by ideal perturbed equilibria, but one must ensure no internal instabilities to trust the results. The internal instabilities can be avoided by better reconstruction of axisymmetric equilibria, but it should be resolved in the future how to treat the intrinsically unstable surfaces such as $q = 1$ in perturbed equilibria.

IV. DEFORMATION OF FLUX SURFACES AND NTV TRANSPORT

As another important consequence by non-axisymmetric perturbations, the deformed magnetic surfaces and the distorted trajectories of particle orbits produce so-called non-ambipolar transport [17–22]. Ions typically diffuse faster, and resulting net radial currents produce toroidal torques which relax the $\vec{E} \times \vec{B}$ rotation to an ambipolar level. Therefore, the non-ambipolar transport causes rotational damping, and the associated viscosity is often called Neoclassical Toroidal Viscosity (NTV) [14, 23–25]. When non-axisymmetric magnetic perturbations are applied to change the toroidal rotation, it is called NTV magnetic braking [40, 41] of rotation in experiments.

A. Variation of field strength

There are various theoretical predictions for NTV that can be compared with experimental damping rates of rotation. Any evaluation requires knowledge of the variation in the field

strength $B = |B|$ and thus the calculation of perturbed equilibrium. This can be understood by considering the action of a trapped particle with given energy H and magnetic moment μ as

$$J = \oint M v_{\parallel} dl \propto \oint \sqrt{H - \mu|B|} dl, \quad (6)$$

where M is the mass of a particle. The action must be conserved for a particle, but the action depends on the toroidal location of the turning points of a trapped particle if B is not axisymmetric. Hence, a trapped particle must drift radially to conserve the action while it precesses toroidally.

The non-axisymmetry in B must be evaluated along the true magnetic field lines dl , which means along perturbed magnetic field lines. The variation in B along the perturbed magnetic field lines is called *Lagrangian* variation in the field strength and is given by [16]

$$\delta_L B = \delta_E B + \vec{\xi} \cdot \vec{\nabla} B_0. \quad (7)$$

On the other hand, the *Eulerian* variation at fixed points in space is

$$\delta_E B = \delta \vec{B} \cdot \hat{b}. \quad (8)$$

The vacuum approximation uses the Eulerian variation, but based on the external field instead of the total field, that is,

$$\delta_E B^x = \delta \vec{B}^x \cdot \hat{b}. \quad (9)$$

The difference of two Eulerian evaluations, $\delta_E B$ and $\delta_E B^x$, depends on plasma response. When plasma response is weak, the two estimations may give roughly similar variations even though the actual field structure will be largely distorted by perturbed plasma currents, as can be seen Figs. 1 and 2. However, the correct variation in the field strength for Eq. (6) is not either of them, but is the Lagrangian variation given by Eq. (7).

The Lagrangian $\delta_L B$ is typically larger than Eulerian variation since it is dominantly determined by spatial variations of $B_0 \propto 1/R$ seen in displaced magnetic field lines by $\vec{\xi}$. The example is shown in Fig. 5, where $n = 1$ field with a typical current $\sim 1kA$ using EFC coils (or called Resistive Wall Mode (RWM) coils) is applied to a NSTX plasma. A moderate $\beta_N = 1.0$ case is chosen to suppress a large amplification, as one can see from that $\delta_E B$ is roughly similar to vacuum approximation $\delta_E B^x$. Although plasma amplification can be ignored in this example, one can still find that the Lagrangian variation is larger than the

vacuum approximation by an order of magnitude. In practice, vacuum approximation gives $\delta_E B^x/B_0 \sim 10^{-4}$ and the Lagrangian evaluation including plasma response gives $\delta_L B/B_0 \sim 10^{-3}$. If the applied field is close to a marginally stable mode, the Lagrangian evaluation can give even larger amplitudes. NTV transport is proportional to $\delta_L B_{mn}^2$, so an order of magnitude change in $\delta_L B_{mn}$ gives a two order of magnitude change in the NTV.

The Lagrangian $\delta_L B$ in IPEC can provide relevant prediction for the variation in the field strength, however, a singularity exists in the narrow region around the rational surfaces. This arises because the tangential displacement is determined by $\vec{\nabla} \cdot \vec{\xi} = 0$ and gives $\xi_{\parallel} \propto \vec{\nabla} \cdot \vec{\xi}_{\perp}/(m - nq)$. This is the feature of ideal perturbed equilibria and can be kept if the evaluation for only a local torque is desired. However, the singularity needs to be removed for the evaluation of the total toroidal torque. IPEC alters the tangential displacement as [42]

$$\xi_{\parallel} \propto \frac{m - nq}{(m - nq)^2 + \sigma^2} \vec{\nabla} \cdot \vec{\xi}_{\perp}, \quad (10)$$

introducing a small parameter σ , which can be reasonably taken as $\sigma_g \approx -n(dq/d\psi)\Delta\psi_g$ with $\Delta\psi_g$ given by an ion gyro-radius. The integration and the total torque are not sensitive to variations of σ , if $\sigma \sim \sigma_g$ within an order of magnitude, since only the very narrow region around the rational surfaces is affected by the small parameter. Although the singularity can be removed with the small parameter, the peaks around the rational surfaces as seen in Fig. 5 may be nonphysical. This is the consequence of the non-self-consistency in ideal perturbed equilibria, which will be briefly discussed later.

B. Theoretical prediction of NTV braking

The variation in the field strength $\delta_L B$ given by IPEC can be used to evaluate NTV torques and rotational damping rates. NTV transport has been studied by a number of authors. In particular, Shaing has calculated various asymptotic limits in perturbed tokamaks including multi-harmonic perturbations [14, 23–25]. It has been known that there are two main regimes, the $1/\nu$ regime [24] when $\omega_E \ll \nu$ and the $\nu\sqrt{\nu}$ regime [25] when $\omega_E \gg \nu$, where ω_E is the toroidal precession angular frequency and ν is the collisional frequency. Although the calculations are more realistic than the previous calculations with a single harmonic perturbation, it is still difficult to apply the results to tokamaks since the calculations in different asymptotic limits differ by several orders of magnitude as they

switch from one regime to another. Also, the precession rates are strong enough for Neutral Beam Injection (NBI)-heated tokamaks to give resonances with bouncing motion of trapped particles. Therefore, a generalized formula has been derived to include precession and resonance effects and combine different regimes [22]. The resonance effects between the electric precession and the bouncing orbits have been calculated in [21] for a single harmonic perturbation, but the generalization in [22] includes multi-harmonic perturbations and combines different regimes using an effective collisional operator. Including the general formula, here two evaluations in the asymptotic limits for the $1/\nu$ regime and the $\nu\text{-}\sqrt{\nu}$ regime, are also summarized for comparison.

The NTV torque can be conveniently expressed by the flux-averaged toroidal force density, $\tau^\varphi \equiv \vec{\tau} \cdot \vec{\nabla} \varphi \equiv \langle \hat{\phi} \cdot \vec{\nabla} \cdot \vec{\Pi}_a \rangle$ for species a , where $\hat{\phi}$ is the unit vector of ordinary toroidal angle. Dropping the species a subscripts, each evaluation gives

$$\tau_{1/\nu}^\varphi = \frac{\epsilon^{3/2} p u_{1/\nu}^\varphi}{\sqrt{2} \pi^{3/2} R_0} \frac{\lambda_i}{\nu} \int_0^1 d\kappa^2 \delta_{w,1/\nu}^2 \quad (11)$$

$$\tau_{\nu\text{-}\sqrt{\nu}}^\varphi = \frac{\epsilon^{-1/2} p u_{\nu\text{-}\sqrt{\nu}}^\varphi}{\sqrt{2} \pi^{3/2} R_0} \frac{\eta_i}{\omega_E^2} \int_0^1 d\kappa^2 \delta_{w,\nu\text{-}\sqrt{\nu}}^2 \quad (12)$$

$$\tau_\ell^\varphi = \frac{\epsilon^{1/2} p u_\ell^\varphi}{\sqrt{2} \pi^{3/2} R_0} \int_0^1 d\kappa^2 \delta_{w,\ell}^2 \int_0^\infty dx \mathcal{R}_{1,\ell}, \quad (13)$$

for the $1/\nu$, the $\nu\text{-}\sqrt{\nu}$ the and general formula, respectively. The R_0 is the major radius at the magnetic axis, and the parameters are $\lambda_i = 13.718$ and $\eta_i = 0.354$ [24]. The δ_w^2 is the square of variation in the field strength with different weighting factor for different harmonic perturbations.

$$\delta_{w,1/\nu}^2 \equiv \sum_{nmm'} \delta_{nmm'}^2 \frac{n^2 F_{nm0}^{1/2} F_{nm'0}^{1/2}}{E(\kappa) - (1 - \kappa^2)K(\kappa)} \quad (14)$$

$$\delta_{w,\nu\text{-}\sqrt{\nu}}^2 \equiv \sum_{nmm'} \delta_{nmm'}^2 (E(\kappa) - (1 - \kappa^2)K(\kappa)) \quad (15)$$

$$\times \left(\frac{\partial L_{nmc}}{\partial \kappa^2} \frac{\partial L_{nm'c}}{\partial \kappa^2} + \frac{\partial L_{nms}}{\partial \kappa^2} \frac{\partial L_{nm's}}{\partial \kappa^2} \right) \quad (16)$$

$$\delta_{w,\ell}^2 \equiv \sum_{nmm'} \delta_{nmm'}^2 \frac{n^2 F_{nm\ell}^{-1/2} F_{nm'\ell}^{-1/2}}{4K(\kappa)}, \quad (17)$$

where $K(\kappa)$ is the elliptic integral of the first kind, $E(\kappa)$ of the second kind and

$$\delta_{nmm'}^2 = \text{Re}(\delta_{nm})\text{Re}(\delta_{nm'}) + \text{Im}(\delta_{nm})\text{Im}(\delta_{nm'}), \quad (18)$$

with the field model

$$B = B_0(1 - \epsilon \cos \vartheta) + B_0 \left(\sum_{nm} \delta_{nm} e^{i(m\vartheta - n\phi)} \right). \quad (19)$$

Each function is defined as

$$F_{nm\ell}^y \equiv \int_{-\vartheta_t}^{\vartheta_t} d\vartheta (\kappa^2 - \sin^2(\vartheta/2))^y \cos(m - nq - \sigma\ell)\vartheta \quad (20)$$

$$L_{nmc} \equiv \frac{F_{nm0}^{-1/2}}{2K(\kappa)} \left(1 - \cos(\sqrt{n}\varsigma) e^{-\sqrt{n}\varsigma} \right) \quad (21)$$

$$L_{nms} \equiv \frac{F_{nm0}^{-1/2}}{2K(\kappa)} \left(\sin(\sqrt{n}\varsigma) e^{-\sqrt{n}\varsigma} \right), \quad (22)$$

with the turning point $\vartheta_t \equiv 2 \arcsin(\kappa)$, the sign function σ that +1 for co-rotating case, and the stretch variable related to the width of layer for $\sqrt{\nu}$ regime [25]

$$\varsigma = (1 - \kappa^2) \left(\frac{\ln(16/\sqrt{4\nu/\epsilon\omega_E})}{4\nu/\epsilon\omega_E} \right)^{1/2}. \quad (23)$$

The resonant term in Eq. (13) is given by

$$\mathcal{R}_{1,\ell} = \frac{1}{2} \frac{(1 + (\frac{\ell}{2})^2)^{\frac{\nu}{2\epsilon}} x e^{-x}}{(\ell\omega_b - n(\omega_E + \omega_B))^2 + ((1 + (\frac{\ell}{2})^2)^{\frac{\nu}{2\epsilon}})^2 x^{-3}}. \quad (24)$$

Here the normalized variables (x, κ^2) are used instead of (E, μ) as $x \equiv E/T$ and $\kappa^2 \equiv (E - \mu B_0(1 - \epsilon))/2\mu B_0\epsilon$. The bounce frequency ω_b and the magnetic precession ω_B are functions of (x, κ^2) , but one can use further approximations by making them as functions only of x . The approximations are

$$\omega_b = \frac{\pi\sqrt{\epsilon}}{2\sqrt{2}} \omega_t \frac{\sqrt{x}}{K(\kappa)} \approx \frac{\pi\sqrt{\epsilon}}{4\sqrt{2}} \omega_t \sqrt{x}, \quad (25)$$

$$\omega_B = \sigma \frac{q^3 \omega_t^2}{2\epsilon \omega_g} x \frac{F_{010}^{-1/2}(\kappa)}{4K(\kappa)} \approx \sigma \frac{q^3 \omega_t^2}{4\epsilon \omega_g} x, \quad (26)$$

where the transit frequency $\omega_t = v_t/qR_0$ with the thermal velocity $v_t = (2T/M)^{1/2}$, and the gyrofrequency $\omega_g = eB/M$. The torque is proportional to the toroidal flow $u^\varphi = \vec{u} \cdot \vec{\nabla} \varphi$ with an offset by the neoclassical flow

$$u_N^\varphi \equiv u^\varphi + C_N \sigma \left| \frac{1}{e} \frac{dT}{d\chi} \right|, \quad (27)$$

where the χ is the poloidal flux function. The constants for each regime are $C_{1/\nu} \approx 3.5$, $C_{\nu-\sqrt{\nu}} \approx 0.92$, and $C_\ell \approx 2.0$.

The general formula in Eq. (13) with $\ell = 0$ approximates well the $1/\nu$ asymptotic limit in Eq. (11) when $\omega_E + \omega_B \rightarrow 0$, and also roughly approximate $\nu\sqrt{\nu}$ asymptotic limit in Eq. (12) when $\nu \rightarrow 0$, although it can underestimate the effects of non-resonant harmonic perturbations. In order to correct the underestimation, one take a maximum $\tau^\varphi = \max\{\ell|\tau_\ell^\varphi, \tau_{\nu\sqrt{\nu}}^\varphi\}$. However, the present formula for $\nu\sqrt{\nu}$ in Eq. (11) is highly sensitive to the width of the layer in Eq. (23), which largely changes throughout the plasma volume. The underestimation is not so large unless ν is smaller than $10^3/s$ [22], so here the general formula in Eq. (13) with $\ell = 0$ is used to approximate $\nu\sqrt{\nu}$. Since $\ell = 0$ means the rough connection between the $1/\nu$ and the $\nu\sqrt{\nu}$ regime, it can be called $1/\nu\nu$ evaluation. Also, the inclusion of all ℓ bounce harmonics dominates $\nu\sqrt{\nu}$ in most cases, the evaluation using the general formula can be made by $\tau^\varphi = \max\{\ell|\tau_\ell^\varphi\}$ on each flux surface, or simply by $\tau^\varphi = \sum \tau_\ell^\varphi$ since only one of τ_ℓ^φ is largely dominant on a flux surface.

The Eqs. (11) to (27) can be used only for approximations due to the following limitations : (1) The evaluations take only trapped particles into account since the effects by passing particles are expected to be weaker than trapped particles. This can be checked by comparing the $1/\nu$ evaluation for trapped particles and the collisional [23] or plateau [43] evaluations for passing particles [40], when precession or resonance are ignored. However, a systematic evaluation for the effects of passing particles in the presence of the precessions has not been done yet. (2) The field model in Eq. (19) ignores a high-order shaping terms of plasmas assuming a high aspect-ratio circular tokamak. Although the model can describe effectively the width and the depth of magnetic wells, present tokamaks typically have strong shaping and so NTV evaluations can be inaccurate especially in the edge. Also, the use of the simplified ω_b or ω_B as only a function of the energy x can be inaccurate for the resonant term in Eq. (24). These simplifications are used for an order of magnitude estimation without computationally demanding process, since (3) the analytic treatment anyway cannot exactly describe complicated dynamics of trapped particles that may lead to stochastic transport [19]. These limitations have to be resolved by numerical evaluations, for instance, using δf code, in the future.

C. Experimental measurement of NTV braking

The Eqs. (11) to (27) give various expressions for the toroidal torque, which can be compared with experiments. While making comparisons between theory and experiment, it is convenient to use rotational damping rates as

$$\nu_{damp} \cong \frac{\tau^\varphi}{u^\varphi R_0 MN}, \quad (28)$$

where N is the density of a species.

Fig. 6. shows $n = 3$ magnetic braking experiments performed in NSTX. The two shots have almost identical plasmas, run in lower single null configuration, with elongation as high as $\kappa = 2.3$, with $I_p = 800kA$ (Fig. 6 (a)) and $B_{T0} = 0.45T$. The electron densities are similar to each other (Fig. 6 (b)). For one of these shots, $n = 3$ braking field is applied using EF/RWM coils in NSTX with currents $600A$ for each (Fig. 6 (c)). One can see from (b) that the amplitude of the braking is low enough not to significantly change the particle confinement. However, a clear change was made in momentum confinement [44]. The plasma rotation reached up to $20 \sim 30kHz$ in the early period by $6MW$ NBI and settled down to similar rotational equilibrium as shown in Fig. 6 (d). However, when the braking field is fully applied at $t = 500ms$, the toroidal rotation starts to damp and relaxes to a different rotational equilibrium. This example indicates the non-ambipolar transport by non-axisymmetric field can produce a strong momentum transport, but the particle confinement is not significantly modified.

The use of a reference shot in magnetic braking is important to discriminate the effects by the non-ambipolar transport. The change of toroidal rotation is determined not only by the non-ambipolar transport with perturbations, but also by various sources including the turbulence-driven momentum transport [45] and the input torque by NBI. The momentum balance equation can be roughly written as

$$MN \frac{\partial u_\phi}{\partial t} = \langle \hat{\phi} \cdot \delta \vec{j} \times \delta \vec{B} \rangle - \langle \hat{\phi} \cdot \vec{\nabla} \cdot \vec{\Pi} \rangle \quad (29)$$

$$+ \frac{\partial}{\partial \rho} \left(MN \chi_\phi \frac{\partial u_\phi}{\partial \rho} - MN u^{pinch} u_\phi \right) + S, \quad (30)$$

for the time evolution of the toroidal rotation $u_\phi = \vec{u} \cdot \hat{\phi}$, where ρ is an effective minor radius. The first term in the right hand side is the torque at the rational surfaces due to the shielding currents, and is related to locking. The second term is the non-ambipolar torque

given by magnetic braking. The third term includes a diffusive process (χ_ϕ) of the transport and a pinch (u^{pinch}) [45], both of which can include classical, neoclassical and turbulence driven momentum transport. The last term represents the torque due to heating sources by NBI. The best way to discriminate the second term in experiments is to use a reference shot that can be subtracted from a magnetic braking shot. The plasma condition must be almost identical, and one must determine the damping in a short time period, otherwise the different rotation rate can modify other terms in Eq. (30). When the time period is short, the exponential decay of the rotation to a new rotational equilibrium can be linearized. In NSTX, the experimental rotational damping rates are measured in this way. The time period is as short as $\sim 50ms$, beyond which the linear behavior can not be assumed.

Fig. 7 shows the evolutions of the rotation mapped on the flux surfaces, with and without $n = 3$ magnetic braking. One can see the profile of the toroidal rotation is almost identical before the magnetic braking ($t = 500ms$), but evolves differently after the magnetic braking, so one can subtract (a) from (b) to obtain the damping purely driven by the braking. In this example, the rotation does not evolve very much without the braking, but this is not seen for all the cases, and it is better to find and use an identical reference shot.

There are other issues in the comparison with the observed damping rates. The toroidal rotation in NSTX (and DIII-D) is measured by CHarge Exchange Recombination Spectroscopy (CHERS) based on the Carbon impurities. Here it will be assumed that the CHERS measurement represents the toroidal rotation of the main ions, as is commonly assumed in experiments. However, since a certain amount of time is required to achieve the equilibration between carbon ions and main (deuterium) ions, a damping seen by CHERS can have smoother profiles than the immediate response of the main ions. These effects are ignored in our study, but should be addressed.

D. Comparison between theory and experiment

The measured damping rates purely by the magnetic braking can be compared with the NTV calculations using the IPEC field. There have been different methods, for instance, using a $1/\nu$ regime and the external (vacuum) field, which have been often successful to approximate the observed damping rates in NSTX [40]. Here three additional physics are included to improve the consistency between theory and experiment :

- (a) Toroidal precession rates ($\omega_p = \omega_E + \omega_B$), which are often faster than the collisional rates (ν).
- (b) The bouncing orbits of trapped particles can resonate with the precessions, that is, $\ell\omega_b \sim n\omega_p$.
- (c) Variation of field strength along the perturbed magnetic field lines, that is, $\delta_L B$, including plasma response is substantially different from vacuum approximation $\delta_E B^x$.

As in the Fig. 8, one can obtain different results if

- (1) (a), (b) and (c) are all ignored : vacuum $1/\nu$
- (2) (a) is only included : vacuum $1/\nu_{\nu}$ ($\ell = 0$)
- (3) (a) and (b) are included : vacuum general (all ℓ)
- (4) (a), (b) and (c) are all included : IPEC general (all ℓ)

The evaluation assuming $1/\nu$ regime based on vacuum approximation can be close to measurement (vacuum $1/\nu$) as presented in [40]. However, the inclusion of the strong precession gives too small damping rates (vacuum $1/\nu_{\nu}$) even if the method is more consistent with theory, unless the bounce-harmonic resonances (vacuum general) and the true variation in the field strength are considered (IPEC general).

Fig. 8 shows that the general NTV including bounce-harmonic resonances coupled with $\delta_L B$ can significantly improve the consistency between theory and experiment, but also shows that the accuracy is still not sufficient to predict the detailed profile of damping rates. Fig. 9 showed other comparisons for the damping rates between measurements and NTV calculations, in NSTX and DIII-D experiments. One can see that predictions are valid only within an order of magnitude. The investigated shots in Fig. 9 are not so different from each other in both devices, but the predictions can show easily an-order-of-magnitude difference, as is obviously seen in Fig. 9 (b).

As is known in ideal stability analysis, ideal perturbed equilibria can be sensitive to the p and q profiles [30], especially in high β_N plasmas. The application of ideal perturbed equilibria to NTV transport provides indeed a rigorous test on the sensitivity, since the difference in the perturbed field and the displacement $\delta_L B$ is amplified through $\tau^\varphi \propto (\delta_L B)^2$.

Although the investigated cases are based on the reasonably accurate equilibrium reconstructions, with the q profiles using Motional Stark Effect (MSE) measurements in both NSTX and DIII-D, a nontrivial sensitivity still exists in the results. This sensitivity of ideal perturbed equilibria on the equilibrium reconstruction must be carefully investigated in the future. Also, one can notice that the predictions are particularly inaccurate in the edge. Although the large damping rates in the predictions are partially due to $u^\varphi \approx 0$ in the edge, the overestimated damping rates compared to the experiments are mainly due to the large Lagrangian variation in the field strength. The results indicate that the ideal constraints may not hold in the edge, and non-ideal effects such as the destroyed flux surfaces by islands and the currents associated with the large torques should be included in perturbed equilibria.

V. NON-SELF-CONSISTENCY IN IDEAL PERTURBED EQUILIBRIA

Ideal perturbed equilibria describe perturbed plasmas with shielded islands by parallel currents and with deformed magnetic surfaces. An inconsistency occurs when ideal perturbed equilibria are used to describe torque effects, since there is no toroidal torque in scalar pressure equilibria. A mathematical identity implies that the torque between any two constant pressure surfaces vanishes $\int(\vec{x} \times \vec{\nabla} p) d^3x = 0$. For consistency, one must solve tensor pressure perturbed equilibria $\vec{\nabla} p + \vec{\nabla} \cdot \vec{\Pi} = \vec{j} \times \vec{B}$ [15]. However, if the torques are sufficiently small, ideal perturbed equilibria can be a valid approximation.

The validity can be theoretically argued by estimating the total energy δW and the total torque $T_\phi = \int(\vec{x} \times \tau^\varphi) d^3x$, produced by non-axisymmetric perturbations. It is convenient to use the dimensionless quantities

$$s \equiv -\frac{\delta W}{\delta W_v} \quad \text{and} \quad \alpha \equiv -\frac{T_\phi}{2\delta W_v}, \quad (31)$$

where δW_v is the required energy to produce the same perturbation, but without plasma [46]. The comparison between s and α gives the importance of the toroidal torque when calculating perturbed equilibria. An ideal perturbed equilibria can be valid when $|s| > |\alpha|$. The s is automatically given by IPEC, and the α can be approximately given by estimating the generalized NTV torque using Eq. (13). When islands are ignorable, the NTV torque dominates the drive for the rotational damping [40]. The $n = 3$ application shown in Fig.

8 has $|s| \sim 0.3 < |\alpha| \sim 0.5$. This example implies that the effects by torque on perturbed equilibria are substantial, as can be seen by the largely overestimated damping rates in the edge. The $n = 3$ applications shown in Fig. 9 have $|s| > 0.5$ and $|\alpha| < 0.2$, which indicate that ideal perturbed equilibria can be valid in principle. However, these estimations based on the (s, α) model only give the importance of the torque in total, but not for a local torque. The nonphysical peaks in the $\delta_L B$ in Fig. 5 and the NTV torques in Figs. 8 and 9 still imply the importance of local torques in the calculations of perturbed equilibria. Also, the inclusion of the currents associated with the torque would improve the largely overestimated damping rates in the edge, which can change the penetration of the field throughout the plasma.

The apparent breakdown in ideal approximation can occur when the plasma approaches to a marginally stable point, since then $s \rightarrow 0$, which makes amplification easier and thus increases α . The large torque up to $|\alpha| \sim |s|$ implies the phase shift of the plasma response [46], and then the perturbation can no longer tap the energy from the plasma. When $|\alpha| \sim |s|$, the shielding by currents associated with the torque has been theoretically expected [46–48], and also from recent NSTX observations based on the single (s, α) model [49]. This is important for $n = 1$ feedback control of Resistive Wall Mode in high β_N plasmas. The higher n has the higher marginal β_N , so IPEC results are expected to be better for many of the higher $n \geq 2$ applications. However, tensor pressure perturbed equilibria are necessary to improve the predictions for more accurate plasma response effects.

VI. CONCLUDING REMARKS

The characteristics of perturbed tokamak equilibria and the importance of ideal plasma response are described. The Ideal Perturbed Equilibrium Code (IPEC) solves perturbed tokamak equilibria with deformed magnetic surfaces but no magnetic islands. IPEC has shown that the effects by perturbed plasma currents can significantly alter the penetration of magnetic perturbations through shielding, amplification and poloidal coupling. The applications to locking experiments in both NSTX and DIII-D have shown the importance of plasma response to understand the observations, and an improved approach using the weighted resonant field including ideal plasma response. This method could be used to give more reliable correction of the intrinsic error field and the prediction of error field threshold

in International Thermonuclear Energy Reactor (ITER) [34].

The importance of plasma response effects is also illustrated with the non-axisymmetric variation of the field strength and consequent non-ambipolar transport and NTV braking. The actual Lagrangian variation in the field strength evaluated along perturbed magnetic field lines is different and typically larger than Eulerian variation along the unperturbed magnetic field lines. When the Lagrangian variation in the field strength in IPEC is coupled with generalized theory of non-ambipolar transport, the consistency between experiment and theory can be improved. However, various unresolved issues remain in both theory and experiment as described.

The present IPEC uses the same method to calculate plasma perturbation as the ideal MHD stability analysis, so the sensitivity also exists to the same extent in the ideal stability of tokamak plasmas. In particular, the result can be sensitive to p and q profiles given by the reconstruction of the experimental equilibrium, so the systematic investigations are required in the future to improve the predictions of plasma response. This sensitivity may be intrinsic since ideal perturbed equilibria ignore the currents associated with tensor pressure, as is obvious when the plasma is close to marginally stable limit. Also, the effects of tensor pressure are important especially in the edge where islands may exist and the currents associated with the torque can be significant. Islands and the NTV transport are the important causes of the toroidal torque, and so the inclusion of a tensor pressure in perturbed equilibria would give a more self-consistent calculation.

This work was supported by DOE contract DE-AC02-76CH03073 (PPPL), DE-FG02-03ERS496 (CU) and DE-FC02-04ER54698 (GA).

-
- [1] T. C. Hender, R. Fitzpatrick, A. W. Morris, P. G. Carolan, R. D. Durst, T. Eddlington, J. Ferreira, S. J. Fielding, P. S. Haynes, J. Hugill, I. J. Jenkins, R. J. La Haye, B. J. Parham, D. C. Robinson, T. N. Todd, M. Valovic, and G. Vayakis, *Nucl. Fusion* **32**, 2091 (1992).
 - [2] R. J. La Haye, R. Fitzpatrick, T. C. Hender, A. W. Morris, J. T. Scoville, and T. N. Todd, *Phys. Fluids B* **4**, 2098 (1992).
 - [3] R. J. Buttery, M. D. Benedetti, D. Gates, Y. Gribov, T. Hender, R.J. La Haye, P. Leahy, J. Leuer, A. Morris, A. Santagiustina, J. Scoville, B. J. D. Tubbing, JET Team, COMPASS-D

- Research Team, and DIII-D Team, Nucl. Fusion **39**, 1827 (1999).
- [4] J. T. Scoville and R. J. LaHaye, Nucl. Fusion **43**, 250 (2003).
- [5] J. E. Menard, M. G. Bell, R. E. Bell, E. D. Fredrickson, D. A. Gates, S. M. Kaye, B. P. LeBlanc, R. Maingi, D. Mueller, S. A. Sabbagh, D. Stutman, C. E. Bush, D. W. Johnson, R. Kaita, H. W. Kugel, R. J. Maqueda, F. Paoletti, S. F. Paul, M. Ono, Y. K. M. Peng, C. H. Skinner, E. J. Synakowski, and the NSTX team, Nucl. Fusion **43**, 330 (2003).
- [6] S. M. Wolfe, I. H. Hutchinson, R. S. Granetz, J. Rice, A. Hubbard, A. Lynn, P. Phillips, T. C. Hender, D. F. Howell, R. J. La Haye, and J. T. Scoville, Phys. Plasmas **12**, 056110 (2005).
- [7] T. E. Evans, R. A. Moyer, P. R. Thomas, J. G. Watkins, T. H. Osborne, J. A. Boedo, E. J. Doyle, M. E. Fenstermacher, K. H. Finken, R. J. Groebner, M. Groth, J. H. Harris, R. J. LaHaye, C. J. Lasnier, S. Masuzaki, N. Ohyabu, D. G. Pretty, T. L. Rhodes, H. Reimerdes, D. L. Rudakov, M. J. Schaffer, G. Wang, and L. Zeng, Phys. Rev. Lett. **92**, 235003 (2004).
- [8] T. E. Evans, R. A. Moyer, J. G. Watkins, T. H. Osborne, P. R. Thomas, M. Becoulet, J. A. Boedo, E. J. Doyle, M. E. Fenstermacher, K. H. Finken, R. J. Groebner, M. Groth, J. H. Harris, G. L. Jackson, R. J. LaHaye, C. J. Lasnier, S. Masuzaki, N. Ohyabu, D. G. Pretty, H. Reimerdes, T. L. Rhodes, D. L. Rudakov, M. J. Schaffer, M. R. Wade, G. Wang, W. P. West, and L. Zeng, Nucl. Fusion **45**, 595 (2005).
- [9] R. A. Moyer, T. E. Evans, T. H. Osborne, P. R. Thomas, M. Becoulet, J. H. Harris, K.-H. Finken, J. A. Boedo, E. J. Doyle, M. E. Fenstermacher, P. Gohil, R. J. Groebner, M. Groth, G. L. Jackson, R. J. LaHaye, C. J. Lasnier, A. W. Leonard, G. R. McKee, H. Reimerdes, T. L. Rhodes, D. L. Rudakov, M. J. Schaffer, P. B. Snyder, M. R. Wade, G. Wang, J. G. Watkins, W. P. West, and L. Zeng, Nucl. Fusion **43**, 330 (2003).
- [10] R. Fitzpatrick and T. C. Hender, Phys. Fluids B **3**, 645 (1991).
- [11] R. Fitzpatrick, Nucl. Fusion **33**, 1049 (1993).
- [12] A. Cole and R. Fitzpatrick, Phys. Plasmas **13**, 032503 (2006).
- [13] A. Cole, C. C. Hegna, and J. D. Callen, Phys. Rev. Lett. **99**, 065001 (2007).
- [14] K. C. Shaing, Phys. Rev. Lett. **87**, 245003 (2001).
- [15] A. H. Boozer and C. Nührenberg, Phys. Plasmas **13**, 102501 (2006).
- [16] A. H. Boozer, Phys. Plasmas **13**, 044501 (2006).
- [17] E. A. Frieman, Phys. Fluids **13**, 490 (1970).
- [18] A. A. Galeev, R. Z. Sagdeev, H. P. Furth, and M. N. Rosenbluth, Phys. Rev. Lett. **22**, 511

- (1969).
- [19] R. J. Goldston, R. B. White, and A. H. Boozer, *Phys. Rev. Lett.* **47**, 647 (1981).
 - [20] R. Linsker and A. H. Boozer, *Phys. Fluids* **25**, 143 (1982).
 - [21] H. E. Mynick, *Nucl. Fusion* **26**, 491 (1986).
 - [22] J.-K. Park, A. H. Boozer, and J. E. Menard, *Phys. Rev. Lett.* **102**, 065002 (2009).
 - [23] K. C. Shaing, *Phys. Fluids* **26**, 3315 (1983).
 - [24] K. C. Shaing, *Phys. Plasmas* **10**, 1443 (2003).
 - [25] K. C. Shaing, P. Cahyna, M. Becoulet, J.-K. Park, S. A. Sabbagh, and M. S. Chu, *Phys. Plasmas* **15**, 082506 (2008).
 - [26] J.-K. Park, A. H. Boozer, and A. H. Glasser, *Phys. Plasmas* **14**, 052110 (2007).
 - [27] A. H. Glasser and M. S. Chance, *Bull. Am. Phys. Soc.* (1997).
 - [28] M. S. Chance, *Phys. Plasmas* **4**, 2161 (1997).
 - [29] A. H. Boozer, *Rev. Mod. Phys.* **78**, 1071 (2004).
 - [30] J. P. Freidberg, *Ideal Magnetohydrodynamics* (Plenum Press, New York, 1993), 338-354.
 - [31] M. Ono, S. Kaye, Y.-K. Peng, G. Barnes, W. Blanchard, M. Carter, J. Chrzanowski, L. Dudek, R. Ewig, D. Gates, R. Hatcher, T. Jarboe, S. Jardin, D. Johnson, R. Kaita, M. Kalish, C. Kessel, H. Kugel, R. Maingi, R. Majeski, J. Manickam, B. McCormack, J. E. Menard, D. Mueller, B. Nelson, C. Neumeyer, G. Oliaro, F. Paoletti, R. Parsells, E. Perry, N. Pomphrey, S. Ramakrishnan, R. Raman, G. Rewoldt, J. Robinson, A. Roquemore, P. Ryan, S. A. Sabbagh, D. Swain, E. Synakowski, M. Viola, M. Williams, J. Wilson, and the NSTX Team, *Nucl. Fusion* **40**, 557 (2000).
 - [32] J. L. Luxon and L. G. Davis, *Fusion Technology* **8**, 441 (1985).
 - [33] J.-K. Park, M. J. Schaffer, J. E. Menard, and A. H. Boozer, *Phys. Rev. Lett.* **99**, 195003 (2007).
 - [34] J.-K. Park, A. H. Boozer, J. E. Menard, and M. J. Schaffer, *Nucl. Fusion* **48**, 045006 (2008).
 - [35] J.-K. Park, A. H. Boozer, and J. E. Menard, *Phys. Plasmas* **15**, 064501 (2008).
 - [36] R. C. Grimm, R. L. Dewar, and J. Manickam, *J. Comput. Phys.* **49**, 94 (1983).
 - [37] M. G. Bell, R. E. Bell, D. A. Gates, S. M. Kaye, H. Kugel, B. P. LeBlanc, F. M. Levinton, R. Maingi, J. E. Menard, R. Raman, S. A. Sabbagh, D. Stutman, and the NSTX team, *Nucl. Fusion* **46**, S565 (2006).
 - [38] S. Hamada, *Nucl. Fusion* **2**, 23 (1962).

- [39] M. J. Schaffer, J. E. Menard, M. P. Aldan, J. M. Bialek, T. E. Evans, and R. A. Moyer, Nucl. Fusion **48**, 024004 (2008).
- [40] W. Zhu, S. A. Sabbagh, R. E. Bell, J. M. Bialek, B. P. LeBlanc, S. M. Kaye, F. M. Levinton, J. E. Menard, K. C. Shaing, A. C. Sontag, and H. Yuh, Phys. Rev. Lett. **96**, 225002 (2006).
- [41] A. M. Garofalo, K. H. Burrell, J. C. Deboo, J. S. deGrassie, G. L. Jackson, M. Lanctot, H. Reimerdes, M. J. Schaffer, W. M. Solomon, E. J. Strait, and the DIII-D team, Phys. Rev. Lett. **101**, 195005 (2008).
- [42] J. P. Freidberg, *Ideal Magnetohydrodynamics* (Plenum Press, New York, 1993), 289-295.
- [43] K. C. Shaing, S. P. Hirshman, and J. D. Callen, Phys. Fluids **29**, 521 (1986).
- [44] S. M. Kaye, W. M. Solomon, R. E. Bell, B. LeBlanc, F. M. Levinton, J. E. Menard, G. Rewoldt, S. A. Sabbagh, W. Wang, and H. Yuh, in *Proceedings of 22nd IAEA Fusion Energy Conference* (IAEA, Geneva, Switzerland, 2008).
- [45] W. M. Solomon, S. M. Kaye, R. E. Bell, B. P. LeBlanc, J. E. Menard, G. Rewoldt, and W. Wang, Phys. Rev. Lett. **101**, 065004 (2008).
- [46] A. H. Boozer, Phys. Rev. Lett. **86**, 5059 (2001).
- [47] A. H. Boozer, Phys. Plasmas **3**, 3375 (1996).
- [48] H. E. Mynick and A. H. Boozer, Phys. Plasmas **15**, 082502 (2008).
- [49] J.-K. Park, A. H. Boozer, J. E. Menard, S. P. Gerhardt, and S. A. Sabbagh, (2009), submitted to Phys. Plasmas.

List of Figures

- 1 (COLOR) The normal field δB_{21} as a function of the radius in a perturbed cylindrical force-free plasma. Each solution is obtained using vacuum superposition (Vacuum), cylindrical force-free equation (Cylinder force-free), and IPEC with virtual surface currents (IPEC). Cylinder force-free and IPEC give the almost identical solution inside the plasma and show significant shielding. $r/a \sim 0.83$ is the $q = 2$ resonant surface (dash), $r/a \sim 1.2$ is the wall. . . . 25

- 2 (COLOR) The normal field δB_{31} as a function of the radius in a perturbed cylindrical force-free plasma. As Fig. 1, each solution is obtained using vacuum superposition (Vacuum), cylindrical force-free equation (Cylinder force-free), and IPEC with virtual surface currents (IPEC). Cylinder force-free and IPEC give the almost identical solution for plasma and show substantial amplification throughout plasma. $r/a \sim 1.04$ is the $q = 3$ resonant surface (dash), $r/a \sim 1.2$ is the wall. 25
- 3 (COLOR) The expected resonant field using EFC $n = 1$ correction (300A) for NSTX intrinsic error field as a function of different toroidal phases of the correction field (#116132, $\beta_N \sim 0.4$). The blue region indicates the experimentally known optimal phase of $n = 1$ correction. The external resonant field in magnetic coordinates with an ordinary toroidal angle (PEST δB_{21}^x), the weighted external resonant field (δB_{21}^x), the weighted total resonant field (δB_{21}) are shown and compared. Note that the opposite results by the PEST δB_{21}^x 26
- 4 (COLOR) The revised figure from Fig.3 in [33] for the critical field versus locking density with the various $n = 1$ DIII-D error field corrections, based on the weighted total (external) resonant field $\delta B_{mn}^{(x)}$. From the left, it is shown that I+M, C+M, M (#124995, $\beta_N \sim 0.5$) in 2006 DIII-D experiments, and M, I+C+M, I+M in 2004 DIII-D experiments (#117380, $\beta_N \sim 0.5$), respectively. I is I-coil correction, C is C-coil correction, and M is Machine error, which is different for 2006 and 2004. The unstable $q = 1$ surface close to the magnetic axis is ignored. The weighted external resonant field δB_{mn}^x is compared with the weighted total resonant field δB_{mn} at $q = 2/1$ and $q = 3/1$ rational surfaces. Note the roughly linear correlation of locking density is restored with δB_{mn} compared to almost no correlated data with δB_{mn}^x 26

5	(COLOR) Comparison for the radial profiles of one component ($m=1, n=1$) of the non-axisymmetric variation in the field strength between Eulerian vacuum ($\delta_E B^x$), Eulerian IPEC ($\delta_E B$) and Lagrangian IPEC ($\delta_L B$) evaluations. The calculation is done with a typical $n = 1$ Error Field and Resistive Wall Mode (EF/RWM) coil current ($\sim 1kA$) to a moderate $\beta_N = 1.0$ NSTX plasma, so plasma amplifications are not strong in this example. However, Lagrangian variation is still larger than other two Eulerian variations.	27
6	(COLOR) Magnetic braking experiments in NSTX. Time evolutions for (a) Plasma current, (b) Electron density, (c) $n=3$ EF/RWM coil current, and (d) Toroidal rotation are shown for plasmas with (red) and without (black) magnetic braking.	27
7	(COLOR) Comparison of the evolution of the rotational profile mapped on the flux surfaces (a) without magnetic braking and (b) with $n = 3$ magnetic braking, for the plasmas in Fig. 6	28
8	(COLOR) Comparisons between measured damping rates (NSTX #124439) and different methods of NTV calculations. (1) $1/\nu$ evaluation using Eq. (11) and vacuum field ($\delta_E B^x$), (2) $1/\nu_{\perp\nu}$ evaluation using $\ell = 0$ Eq. (13) and vacuum field, (3) general evaluation using all ℓ Eq. (13) and vacuum field, and (4) general evaluation using all ℓ Eq. (13) and IPEC field ($\delta_L B$).	28
9	(COLOR) Comparisons of the damping rates as functions of ψ_N between measurements (\square) and general IPEC NTV calculations in (a) NSTX and (b) DIII-D. Each number indicates each shot in experiments.	29

Figures

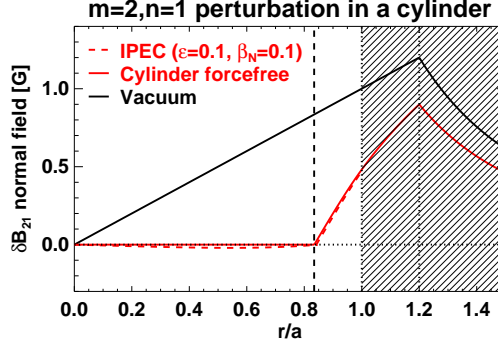


FIG. 1: (COLOR) The normal field δB_{21} as a function of the radius in a perturbed cylindrical force-free plasma. Each solution is obtained using vacuum superposition (Vacuum), cylindrical force-free equation (Cylinder force-free), and IPEC with virtual surface currents (IPEC). Cylinder force-free and IPEC give the almost identical solution inside the plasma and show significant shielding. $r/a \sim 0.83$ is the $q = 2$ resonant surface (dash), $r/a \sim 1.2$ is the wall.

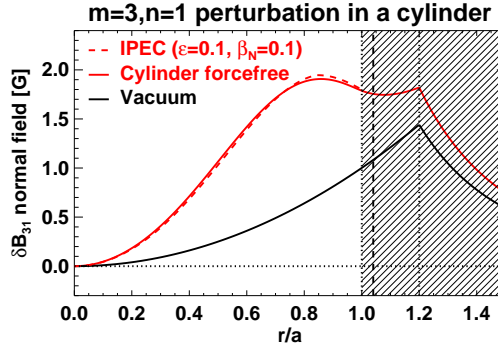


FIG. 2: (COLOR) The normal field δB_{31} as a function of the radius in a perturbed cylindrical force-free plasma. As Fig. 1, each solution is obtained using vacuum superposition (Vacuum), cylindrical force-free equation (Cylinder force-free), and IPEC with virtual surface currents (IPEC). Cylinder force-free and IPEC give the almost identical solution for plasma and show substantial amplification throughout plasma. $r/a \sim 1.04$ is the $q = 3$ resonant surface (dash), $r/a \sim 1.2$ is the wall.

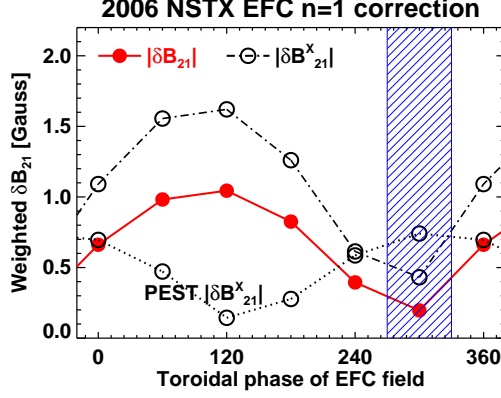


FIG. 3: (COLOR) The expected resonant field using EFC $n = 1$ correction (300A) for NSTX intrinsic error field as a function of different toroidal phases of the correction field (#116132, $\beta_N \sim 0.4$). The blue region indicates the experimentally known optimal phase of $n = 1$ correction. The external resonant field in magnetic coordinates with an ordinary toroidal angle (PEST δB_{21}^x), the weighted external resonant field (δB_{21}^x), the weighted total resonant field (δB_{21}) are shown and compared. Note that the opposite results by the PEST δB_{21}^x .

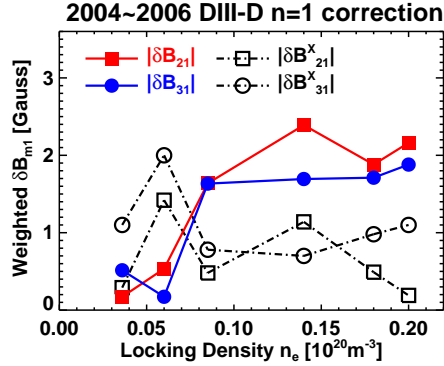


FIG. 4: (COLOR) The revised figure from Fig.3 in [33] for the critical field versus locking density with the various $n = 1$ DIII-D error field corrections, based on the weighted total (external) resonant field $\delta B_{mn}^{(x)}$. From the left, it is shown that I+M, C+M, M (#124995, $\beta_N \sim 0.5$) in 2006 DIII-D experiments, and M, I+C+M, I+M in 2004 DIII-D experiments (#117380, $\beta_N \sim 0.5$), respectively. I is I-coil correction, C is C-coil correction, and M is Machine error, which is different for 2006 and 2004. The unstable $q = 1$ surface close to the magnetic axis is ignored. The weighted external resonant field δB_{mn}^x is compared with the weighted total resonant field δB_{mn} at $q = 2/1$ and $q = 3/1$ rational surfaces. Note the roughly linear correlation of locking density is restored with δB_{mn} compared to almost no correlated data with δB_{mn}^x .

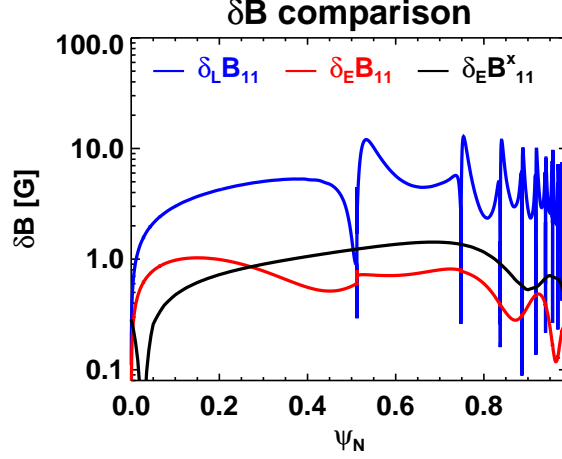


FIG. 5: (COLOR) Comparison for the radial profiles of one component ($m=1, n=1$) of the non-axisymmetric variation in the field strength between Eulerian vacuum ($\delta_E B^x$), Eulerian IPEC ($\delta_E B$) and Lagrangian IPEC ($\delta_L B$) evaluations. The calculation is done with a typical $n = 1$ Error Field and Resistive Wall Mode (EF/RWM) coil current ($\sim 1kA$) to a moderate $\beta_N = 1.0$ NSTX plasma, so plasma amplifications are not strong in this example. However, Lagrangian variation is still larger than other two Eulerian variations.

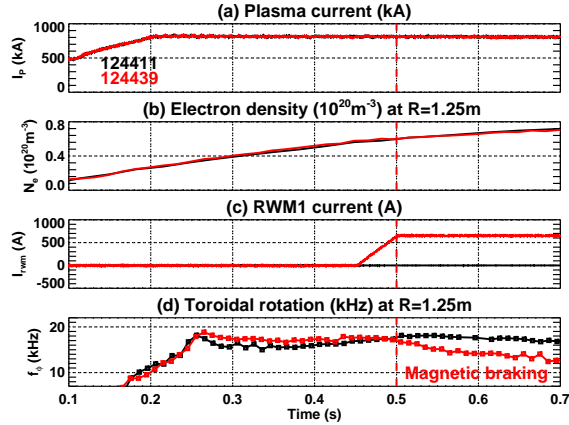


FIG. 6: (COLOR) Magnetic braking experiments in NSTX. Time evolutions for (a) Plasma current, (b) Electron density, (c) $n=3$ EF/RWM coil current, and (d) Toroidal rotation are shown for plasmas with (red) and without (black) magnetic braking.

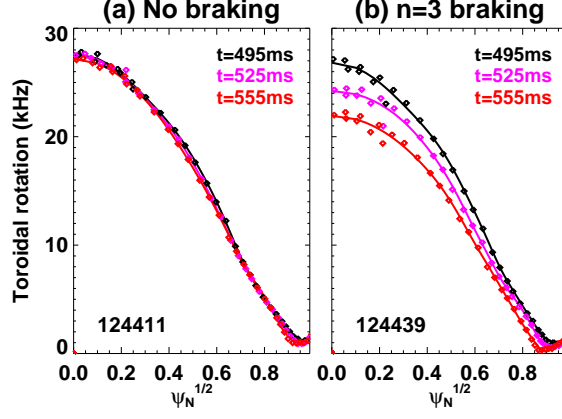


FIG. 7: (COLOR) Comparison of the evolution of the rotational profile mapped on the flux surfaces (a) without magnetic braking and (b) with $n = 3$ magnetic braking, for the plasmas in Fig. 6

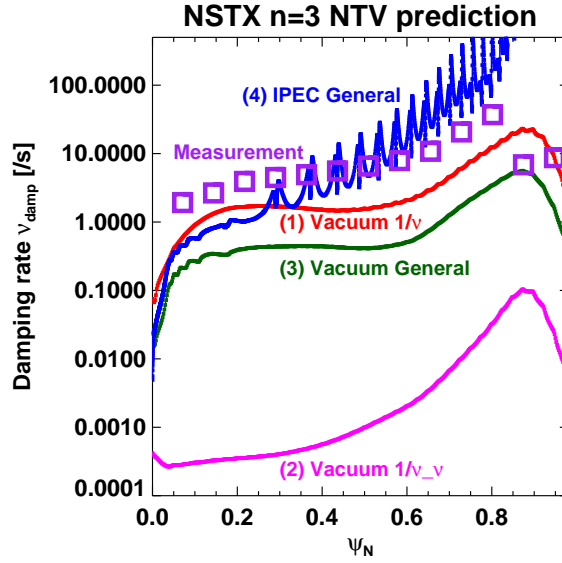


FIG. 8: (COLOR) Comparisons between measured damping rates (NSTX #124439) and different methods of NTV calculations. (1) $1/\nu$ evaluation using Eq. (11) and vacuum field ($\delta_E B^x$), (2) $1/\nu_\nu$ evaluation using $\ell = 0$ Eq. (13) and vacuum field, (3) general evaluation using all ℓ Eq. (13) and vacuum field, and (4) general evaluation using all ℓ Eq. (13) and IPEC field ($\delta_L B$).

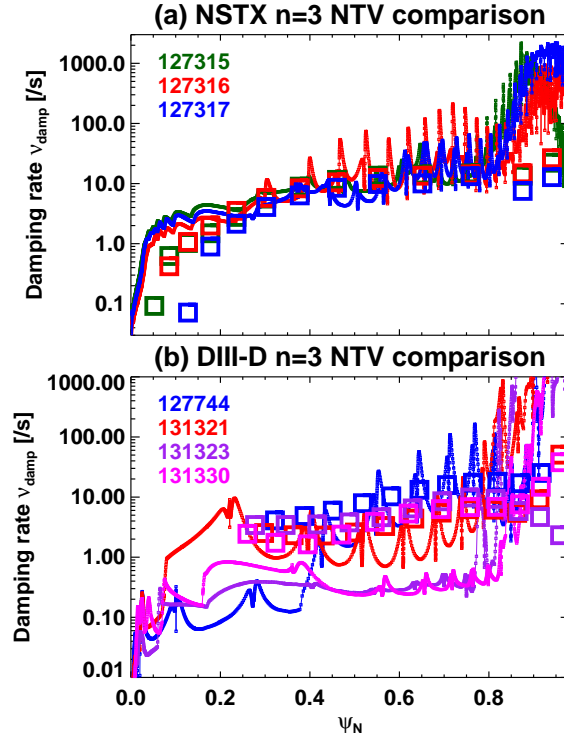


FIG. 9: (COLOR) Comparisons of the damping rates as functions of ψ_N between measurements (\square) and general IPEC NTV calculations in (a) NSTX and (b) DIII-D. Each number indicates each shot in experiments.

The Princeton Plasma Physics Laboratory is operated
by Princeton University under contract
with the U.S. Department of Energy.

Information Services
Princeton Plasma Physics Laboratory
P.O. Box 451
Princeton, NJ 08543

Phone: 609-243-2750
Fax: 609-243-2751
e-mail: pppl_info@pppl.gov
Internet Address: <http://www.pppl.gov>